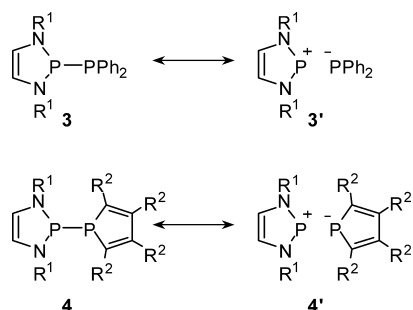


\AA^7) and the diphosphine **2** ($\text{P}-\text{P}$ 2.310 \AA^8), which all show bond lengths that are substantially larger than standard distances ($\text{Si}-\text{Si}$ 2.359(12) \AA , $\text{P}-\text{P}$ 2.214(22) \AA^2). The interest in studies of sterically distorted or electronically highly polarized molecules not only results from the intent to probe the flexibility of the chemical bond but also is motivated by the realization that unusual geometrical structures often trigger unprecedented chemical reactivities or physical properties that are hardly known for undistorted molecules.⁹ For example, whereas diphosphines and disilanes are usually thermally quite stable molecules, **1** and **2** react easily under homolytic cleavage of the central single bond to give persistent radicals.^{8,10} However, although the ease of radical formation is undoubtedly connected with the bond lengthening, it is worth recalling that the exceptional reactivity of **2** is connected with a plethora of structural distortions rather than a single influence,⁸ thus illustrating that no precise understanding of the unusual chemical reactivity can be gained without a detailed analysis of the electronic and geometric distortions.

Earlier, we have reported on the synthesis and characterization of unsymmetrically substituted diphosphines **3** and **4** (Chart 2),

Chart 2



which exhibit $\text{P}-\text{P}$ bonds of similar or even greater length as **2**^{11,12} and undergo at very mild reaction conditions the diphosphination of alkynes and alkenes^{11,13} and metal-assisted activation of nitriles.¹² The origin of this unique reactivity was attributed to distortion of the electronic structure of these molecules and has been described in terms of bond/no-bond resonance between covalent (**3/4**) and ionic (**3'/4'**) canonical structures.^{11,12} Contribution of ionic canonical structures is particularly pronounced in **4/4'** as a result of aromatic stabiliza-

tion in both the cationic N -heterocyclic phosphonium¹⁴ and the anionic phospholyl fragment¹⁵ and induces a particularly strong polarization and prominent lengthening of the $\text{P}-\text{P}$ bonds. However, although this picture seems to provide a qualitative explanation for the observed structural features and reactivity of **4**, more insight is needed to decide if steric interference between peripheral substituents contributes to the distortion (as in **1** and **2**) and to what extent the bond polarization is amenable to fine-tuning by modification of these substituents. In view of the fact that we have recently demonstrated that lengthening of phosphorus-halogen bonds in N -heterocyclic halophosphines is strongly influenced by intermolecular interactions in the crystalline state,¹⁶ it remains also open if the bond lengthening in the diphosphines **4** persists in solution and can thus provide a viable explanation for the observed reactivity.

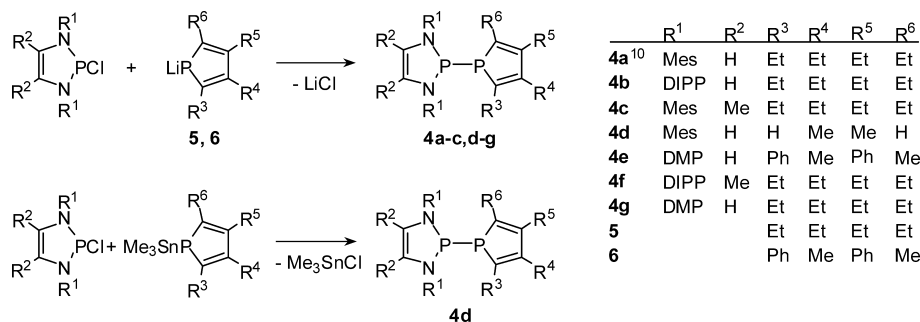
Trying to answer these questions requires gathering structural information on molecules in solution or in the gas phase which can then be compared with data available from single-crystal X-ray diffraction studies. Direct structure elucidation of isolated molecules by gas phase electron diffraction or X-ray absorption spectroscopy is unfeasible owing to the low volatility of the substrates or the lack of suitable heavy atoms. However, Kessler et al.¹⁷ demonstrated a long time ago in a pioneering study that comparison of solid-state and solution NMR data can offer an alternative approach to match molecular structures in solution and solid state. We have now set out to perform a comprehensive study of diphosphines of type **4** in order to gain deeper insight into the origin of the structural distortion and its regulation by modification of substituents at the central framework. To this end, a series of diphosphines was synthesized and characterized by single-crystal X-ray diffraction. NMR studies were conducted in the solid state and in solution and sensitively probe the electronic structure. Analysis of J -couplings and magnetic shielding data allowed to assess the quality of quantum chemical calculations which are used to derive structure-property correlations and enlighten the bonding situation.

Results and Discussion

Syntheses. Diphosphines **4b-f** are accessible straightforwardly from N -heterocyclic chlorophosphines either in the same way as **4a**¹¹ via salt metathesis with lithium phospholides **5** and **6**¹⁸ or via dechlorostannylation with a P -stannyl-phosphole (Scheme 1). The phospholide **6** was prepared for the first time following the known procedure reported for **5**.¹⁸ The reaction leading to this product is remarkable as it represents the first case where coupling of unsymmetrically substituted alkynes on a zirconium template and subsequent metathesis with phosphorus trichloride yields an unsymmetrically substituted chloro-

- (7) Wiberg, N.; Schuster, H.; Simon, A.; Peters, K. *Angew. Chem.* **1986**, *98*, 100; *Angew. Chem., Int. Ed.* **1986**, *25*, 79.
 (8) (a) Hinchley, S. L.; Morrison, C. A.; Rankin, D. W. H.; Macdonald, C. L. B.; Wiacek, R. J.; Cowley, A. H.; Lappert, M. F.; Gundersen, G.; Clyburne, J. A. C.; Power, P. P. *Chem. Commun.* **2000**, 2045. (b) Hinchley, S. L.; Morrison, C. A.; Rankin, D. W. H.; Macdonald, C. L. B.; Wiacek, R. J.; Voigt, A.; Cowley, A. H.; Lappert, M. F.; Gundersen, G.; Clyburne, J. A. C.; Power, P. P. *J. Am. Chem. Soc.* **2001**, *123*, 9045.
 (9) Bock, H.; Ruppert, K.; Näther, C.; Havlas, Z.; Herrmann, H.-F.; Arad, C.; Göbel, I.; John, A.; Meuret, J.; Nick, S.; Rauschenbach, A.; Seitz, W.; Vaupel, T.; Solouki, B. *Angew. Chem.* **1992**, *104*, 564; *Angew. Chem., Int. Ed.* **1992**, *31*, 550.
 (10) Masters, S. L.; Grassie, D. A.; Robertson, H. E.; Hoelbling, M.; Hassler, K. *Chem. Commun.* **2007**, 2618.
 (11) (a) Burck, S.; Gudat, D.; Nieger, M. *Angew. Chem.* **2004**, *116*, 4905; *Angew. Chem., Int. Ed. Engl.* **2004**, *43*, 4801 (CCDC-232848). (b) Burck, S.; Hajdók, I.; Nieger, M.; Bubrin, D.; Schulze, S.; Gudat, D. *Z. Naturforsch.* **2009**, *64b*, 63.
 (12) (a) Burck, S.; Gudat, D.; Nieger, M. *Angew. Chem.* **2007**, *119*, 2977; *Angew. Chem., Int. Ed.* **2007**, *46*, 2919. (b) Burck, S.; Gudat, D.; Nieger, M. *Organometallics* **2009**, *28*, 1447.
 (13) Hajdók, I.; Lissner, F.; Nieger, M.; Strobel, S.; Gudat, D. *Organometallics* **2009**, *28*, 1644.

- (14) Tuononen, H. M.; Roesler, R.; Dutton, J. L.; Ragogna, P. J. *Inorg. Chem.* **2007**, *46*, 10693.
 (15) Nyulászi, L. *Chem. Rev.* **2001**, *101*, 1229.
 (16) Burck, S.; Gudat, D.; Nieger, M.; Benkő, Z.; Nyulászi, L.; Szieberth, D. *Z. Anorg. Allg. Chem.* **2009**, *635*, 245.
 (17) Kessler, H.; Zimmermann, G.; Förster, H.; Engel, J.; Oepen, G.; Sheldrick, W. S. *Angew. Chem.* **1981**, *93*, 1085; *Angew. Chem., Int. Ed. Engl.* **1981**, *20*, 1053.
 (18) (a) Nief, F.; Mathey, F. *Chem. Comm.* **1988**, *12*, 770. (b) Douglas, T.; Theopold, K. H. *Angew. Chem.* **1989**, *101*, 1394; *Angew. Chem., Int. Ed. Engl.* **1989**, *28*, 1367. (c) Westerhausen, M.; Gückel, C.; Warchhold, M.; Nöth, H. *Organometallics* **2000**, *19*, 2393.
 (19) (a) Visseaux, M.; Nief, F.; Ricard, L. *J. Organomet. Chem.* **2003**, *647*, 139. (b) Nief, F.; Turcitu, D.; Ricard, L. *Chem. Commun.* **2002**, *15*, 1646. (c) Turcitu, D.; Nief, F.; Ricard, L. *Chem.-Eur. J.* **2003**, *9*, 4916. (d) Westerhausen, M.; Digeser, M. H.; Gückel, C.; Nöth, H.; Knizek, J.; Ponikvar, W. *Organometallics* **1999**, *18*, 2491.

Scheme 1. Synthesis of Diphosphines^a

^a DMP = 2,6-dimethylphenyl, DIPP = 2,6-diisopropylphenyl.

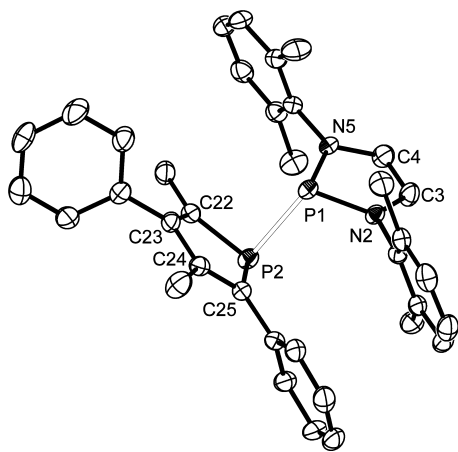


Figure 1. Molecular structure of **4e** (H-atoms were omitted for clarity; 50% probability ellipsoids). Selected bond lengths (Å) and angles (deg) are given in Table 2 and as Supporting Information.

phosphole rather than the usually observed¹⁹ symmetrical products featuring the larger substituents in 2,5-position of the ring.

Crude diphosphines were isolated after removal of formed salts by filtration and evaporation of solvents and were purified by crystallization. All compounds were obtained in good yields as yellow to orange, highly moisture-sensitive, crystalline materials. The solids dissolved readily in anhydrous toluene or hexanes to give thermally stable solutions that decomposed rapidly via P–P bond hydrolysis¹¹ upon exposure to moist air or addition of moist solvents. Pure diphosphines were characterized by analytical and spectroscopic data and (with exception of **4g**) by single-crystal X-ray diffraction studies.

X-ray Diffraction Studies. All crystals studied were composed of well-separated molecules that displayed no specific intermolecular interactions. Representations of the molecular structures of **4e** and **4f** are shown in Figures 1 and 2 (depictions of all molecules and a comprehensive set of data are included as Supporting Information). A summary of X-ray crystallographic data of **4b–f** is given in Table 1, and selected geometrical data of **4a–f** are listed in Table 2. The crystal structure of **4f** is remarkable as the unit cell contains two crystallographically independent molecules (denoted as #1 and #2) that are distinguished by perceptible differences in P–P bond lengths and relative orientations of the phosphole and diazaphospholene rings (Figure 2, Table 4).

Comparison of the structural data reveals that all molecules share a similar *anti* orientation of the two five-membered rings at the central P–P bond and exhibit no significant deviations

in endocyclic bond lengths. The peripheral substituents display no peculiarities. The P–N (1.699–1.728 Å), C–N (1.396–1.415 Å), and C=C bonds (1.321–1.335 Å) in the *N*-heterocyclic rings are similar as in *N*-heterocyclic *P*-hydrido-phosphines and reveal a more prominent bond order alternation, and thus a less pronounced π -electron delocalization, than the corresponding *P*-chloro derivatives.²⁰ The P–C (1.769–1.804 Å), C=C (1.360–1.377 Å), and C–C bond lengths (1.434–1.451 Å) in the phosphole rings lie in the known ranges found for other phospholes and η^1 -phospholyl complexes (P–C 1.79 ± 0.07 Å, C=C 1.36 ± 0.07 Å, C–C 1.46 ± 0.06 Å²¹) and indicate that the π -electron structure in this ring is likewise closer to that of a conjugated diene rather than a delocalized aromatic heterocycle.

Apart from these similarities, there is a considerable variation in the P–P bond distances as well as in certain angular coordinates defining the relative orientation of diazaphospholene and phosphole rings of **4a–f** (see Table 2). The P–P bonds range from 2.356 Å (**4d**) to 2.701 Å (**4c**) and are thus not only much longer than a standard single bond (2.214 ± 0.022 Å²) but can even exceed the distances of 2.427–2.634 Å found for compounds with “one-electron bonds” where two phosphorus atoms are formally connected by a single bonding electron.²² The P(1)–P(2)–C bond angles centered at the P(2) atom of the phosphole ring vary between 79° in **4c** and 89° in **4d** (and hence the angles β_1 between phosphole rings and P–P bonds between 72° and 88°, Table 2); since the endocyclic C–P(2)–C angles in the phosphole rings are always close to 90°, the sum of bond angles at P(2) remains lower than 270°. Sums of valence angles of this magnitude are very rare in phosphine derivatives unless the phosphorus atom is part of a three- or fused four-membered ring system and had otherwise only been found in some phosphanorbornadienes featuring a bridgehead phosphorus atom.²³ A similar pattern as for the changes in bond angles around P(2) is also seen for P(1); here, the endocyclic

(20) Burck, S.; Gudat, D.; Näntinen, K.; Nieger, M.; Niemeyer, M.; Schmid, D. *Eur. J. Inorg. Chem.* **2007**, 5112.

(21) The given numbers indicate the average bond distance ± 3 standard deviations obtained as results of a query in the CSD data base.

(22) (a) Canac, Y.; Bourissou, D.; Baccaredo, A.; Gornitzka, H.; Schoeller, W. W.; Bertrand, G. *Science* **1998**, 279, 2080. (b) Kato, T.; Gornitzka, H.; Schoeller, W. W.; Baccaredo, A.; Bertrand, G. *Angew. Chem.* **2005**, 117, 5633; *Angew. Chem., Int. Ed. Engl.* **2005**, 44, 5497.

(23) (a) Mathey, F.; Mercier, F.; Charrier, C.; Fischer, J.; Mitschler, A. *J. Am. Chem. Soc.* **1981**, 103, 4595. (b) Lelievre, S.; Mercier, F.; Ricard, L.; Mathey, F. *Tetrahedron Asym.* **2000**, 11, 4601. (c) Frison, G.; Brebion, F.; Dupont, R.; Mercier, F.; Ricard, L.; Mathey, F. *C. R. Chim.* **2002**, 5, 245. (d) Germon, A.; Deschamps, B.; Ricard, L.; Mercier, F.; Mathey, F. *J. Organomet. Chem.* **2005**, 690, 1133. (e) Siutkowski, M.; Mercier, F.; Ricard, L.; Mathey, F. *Organometallics* **2006**, 25, 2585.

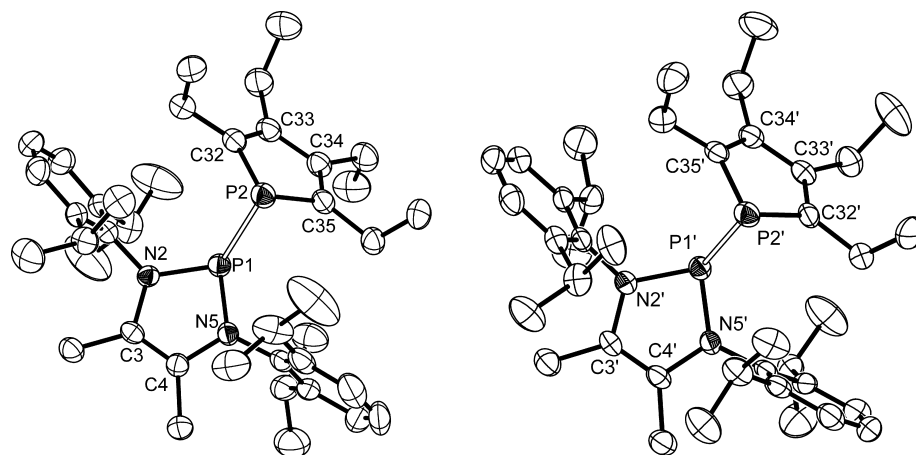


Figure 2. Molecular structure of crystallographically independent molecules **4f#1** (left) and **4f#2** (right) (H-atoms were omitted for clarity; 50% probability ellipsoids). Selected bond lengths (Å) and angles (deg) are given in Table 2 and as Supporting Information.

N–P(1)–N angles remain fixed at $87 \pm 1^\circ$, whereas the average of the two N–P(1)–P(2) angles varies between 103° and 115° (which implies angles β_2 between diazaphospholene ring and P–P bond of 101° in **4d** up to 128° in **4f**), and the sum of angles around P(1) ranges accordingly from 295° to 318° . The individual changes in P–P distances and bond angles show parallel trends, with an increase in bond lengths being accompanied by contraction of P(1)–P(2)–C angles (linear fit of r_{PP} vs the average P(1)–P(2)–C angle gave a correlation coefficient of $R^2 = 0.66$, see Supporting Information) and simultaneous widening of P(2)–P(1)–N angles ($R^2 = 0.74$). As a consequence of these relations, the interplanar angle ϕ between the least-squares planes through the atoms of the diazaphospholene and phosphole rings increases with r_{PP} (linear and quadratic fits of r_{PP} vs ϕ gave correlation coefficients R^2 of 0.77 and 0.92, respectively; cf. Supporting Information), and the diazaphospholene moiety is shifted from a peripheral position, where the P(1) atom is situated above P(2) and both rings are almost parallel, to a point where P(1) is closer to the centroid of the phosphole ring and the two ring planes are distinctly slanted (Figure 3; see also the angle between phosphole ring and P–P bond and the position Δ_P of the projection of the P(1) atom on the phosphole ring plane in Table 2).

However, although the geometrical deviations between **4a–f** are substantial, only part of them can be straightforwardly related to specific intramolecular stereoelectronic influences. Thus, **4d** features the only 2,5-unsubstituted phospholyl moiety, and the finding of the shortest P–P distance may owe to the lack of steric repulsion. The occurrence of particularly long P–P bonds in **4c,f** is presumably induced by the electron-releasing methyl substituents in the *N*-heterocyclic ring, which are known²⁴ to provide inductive stabilization of the diazaphospholenium fragment and may thus enhance the stability of the ionic canonical structure **4'** (Chart 2). In contrast, large deviations in P–P distances between **4a,b** (7 pm), **4c,f** (approximately 15 pm), and even the crystallographically distinguishable specimen **4f#1** and **4f#2** (4 pm) are hardly attributable to substituent effects as replacement of remote methyl groups in *N*-aryl moieties (**4a,b/4c,f**) or merely reorientation of a peripheral ethyl group on the phosphole ring (**4f#1,2**) are not deemed to have significant influence on steric or electronic substituent properties. Thus

ruling out intramolecular effects, one is left with the assumption that intermolecular interactions, commonly denoted as crystal packing effects,^{2b} contribute to the distortions. As the crystal structures give no indication of intermolecular relations other than van der Waals interactions, it must be concluded that even weak forces suffice to induce substantial geometrical distortions of the diphosphines **4**.

To validate this hypothesis, we decided to carry out computational studies on the model compound **7** (Chart 3), which is derived from **4** by replacing *N*-aryl by methyl groups and all other ring substituents by hydrogen atoms. Initial energy optimization of the molecular structure at different levels of theory disclosed a significant dependence of the equilibrium structure on the computational model. Large variations in particular were noted for calculated P–P bond lengths and phosphorus valence angles (Table 3): a trend of shorter P–P distances with the cc-pVDZ basis set and more sophisticated treatment of electron correlation (MP4(SDQ), coupled cluster) was found. Although comparison of computed and experimental bond lengths is problematic because of the absence of peripheral substituents in the model compound and the large spread in bond lengths in **4a–f**, we note that DFT methods with limited basis sets (e.g., the standard B3LYP/6-31G* approach) predict clearly longer bonds than found for **4a,b,d** (which carry no extra methyl groups on *N*-heterocyclic rings), i.e., P–P bond lengths seem to be overestimated. Still, as the use of higher correlated methods and large basis sets was prohibitive for further studies, and since we had in previous investigations on *N*-heterocyclic *P*-halophosphines established^{16,24,25} that DFT methods, regardless of their failure in quantitative predictions of molecular properties, still permit qualitatively correct prediction of trends between similar compounds, we chose the standard B3LYP/6-31G**//B3LYP/6-31G* model for further calculations.

The result of a relaxed scan of the potential energy hypersurface at this level under variation of the P–P distance r_{PP} (Figure 4, top) confirms that the equilibrium geometry resides indeed in a very flat local minimum where even small energetic perturbations permit large geometrical distortions, i.e., less than $0.5 \text{ kcal mol}^{-1}$ of energy are required to induce variation in P–P distances by more than 0.2 \AA . Even if one recalls that this model study permits no quantitative predictions, it still suggests that small intermolecular perturbations (crystal packing effects)

(24) Gudat, D.; Haghverdi, A.; Hupfer, H.; Nieger, M. *Chem.–Eur. J.* **2000**, *6*, 3414.

(25) Burck, S.; Gudat, D. *Inorg. Chem.* **2008**, *47*, 315.

Table 1. Crystallographic Data and Summary of Data Collection and Refinement for 4b–f

	4b	4c	4d
formula	C ₃₈ H ₅₆ N ₂ P ₂	C ₃₄ H ₄₈ N ₂ P ₂	C ₂₆ H ₃₂ N ₂ P ₂
formula weight	602.79	546.68	434.48
T [K]	123(2)	173(2)	123(2)
crystal size (mm ³)	0.50 × 0.30 × 0.20	0.35 × 0.20 × 0.05	0.50 × 0.25 × 0.15
crystal system, space group	monoclinic, <i>P2₁/c</i>	orthorhombic, <i>Pbca</i>	triclinic, <i>P1̄</i>
unit cell dimensions	<i>a</i> = 21.2168(5) Å <i>b</i> = 14.3508(3) Å <i>c</i> = 12.0623(2) Å β = 99.802(1)°	<i>a</i> = 9.2190(2) Å <i>b</i> = 20.3427(5) Å <i>c</i> = 34.1942(9) Å	<i>a</i> = 8.6178(2) Å <i>b</i> = 9.0995(3) Å <i>c</i> = 17.0578(6) Å α = 84.300(2)° β = 77.191(2)° γ = 68.197(2)°
volume (Å ³)	3619.09(13)	6412.8(3)	1210.83(6)
Z, ρ_{calc} (Mg/m ³)	4, 1.11	8, 1.13	2, 1.19
μ (mm ⁻¹)	0.147	0.160	0.195
<i>F</i> (000)	1312	2368	464
θ range for data collection (deg)	2.9–25.0	3.2–25.0	3.1–27.5
completeness of data for θ_{max} (%)	99.8	99.4	96.6
limiting indices	–25 ≤ <i>h</i> ≤ 14, –15 ≤ <i>k</i> ≤ 17, –13 ≤ <i>l</i> ≤ 14	–10 ≤ <i>h</i> ≤ 10, –24 ≤ <i>k</i> ≤ 24, –40 ≤ <i>l</i> ≤ 40	–11 ≤ <i>h</i> ≤ 11, –11 ≤ <i>k</i> ≤ 11, –22 ≤ <i>l</i> ≤ 22
reflections collected/unique	17057/6382 [<i>R</i> _{int} = 0.036]	10474/5628 [<i>R</i> _{int} = 0.105]	20585/5350 [<i>R</i> _{int} = 0.036]
absorption correction	none	none	none
max/min transmission			
data/restraints/parameters	6382/0/379	5628/0/351	5350/0/279
goodness-of-fit on <i>F</i> ²	0.952	1.161	1.062
<i>R</i> 1 [<i>I</i> > 2 σ (<i>I</i>)]	0.038	0.098	0.035
<i>wR</i> 2 <i>R</i> (all data)	0.092	0.183	0.101
largest diff peak and hole (e Å ⁻³)	0.320 and –0.240	0.406 and –0.305	0.251 and –0.306
	4e	4f	
formula	C ₃₆ H ₃₆ N ₂ P ₂	C ₄₀ H ₆₀ N ₂ P ₂	
formula weight	558.61	630.84	
T [K]	123(2)	123(2)	
crystal size (mm ³)	0.30 × 0.20 × 0.10	0.18 × 0.90 × 0.03	
crystal system, space group	monoclinic, <i>P2₁/n</i>	triclinic, <i>P1̄</i>	
unit cell dimensions	<i>a</i> = 8.5577(3) Å <i>b</i> = 26.0553(11) Å <i>c</i> = 13.8925(7) Å β = 95.640(2)°	<i>a</i> = 10.6195(3) Å <i>b</i> = 19.4211(6) Å <i>c</i> = 20.5732(8) Å α = 108.629(2)° β = 95.211(2)° γ = 104.049(2)°	
volume (Å ³)	3082.7(2) Å ³	3834.5(2) Å ³	
Z, ρ_{calc} (Mg/m ³)	4, 1.20 Mg/m ³	4, 1.09 Mg/m ³	
μ (mm ⁻¹)	0.168 mm ⁻¹	0.142 mm ⁻¹	
<i>F</i> (000)	1184	1376	
θ range for data collection (deg)	2.9 to 26.0	3.0 to 25.0°	
completeness of data for θ_{max} (%)	98.1%	99.7%	
limiting indices	–8 ≤ <i>h</i> ≤ 10, –32 ≤ <i>k</i> ≤ 28, –10 ≤ <i>l</i> ≤ 17	–12 ≤ <i>h</i> ≤ 12, –22 ≤ <i>k</i> ≤ 23, –24 ≤ <i>l</i> ≤ 24	
reflections collected/unique	13720/5963 [<i>R</i> _{int} = 0.058]	33389/13516 [<i>R</i> _{int} = 0.068]	
absorption correction	none	none	
max/min transmission			
data/restraints/parameters	5963/0/367	13516/0/797	
goodness-of-fit on <i>F</i> ²	0.903	0.849	
<i>R</i> 1 [<i>I</i> > 2 σ (<i>I</i>)]	0.048	0.053	
<i>wR</i> 2 <i>R</i> (all data)	0.093	0.106	
largest diff peak and hole (e Å ⁻³)	0.332 and –0.285	0.399 and –0.440	

may suffice to induce large variations in P–P bond lengths and that it is a realistic scenario to assume that the spread in P–P distances in **4a–f** is at least in part caused by intermolecular influences rather than intramolecular steric or electronic interactions.

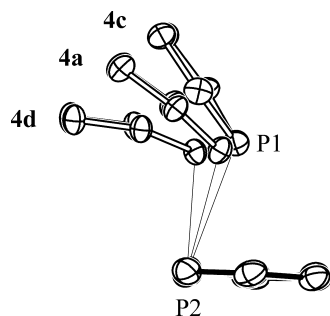
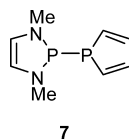
NMR Studies. ³¹P NMR spectra of diphosphines **4a–g** were recorded both in solution and in the solid state. The NMR experiments were used to provide spectroscopic fingerprints of **4a–g**, which were then interpreted with the help of quantum chemical calculations.

The solution spectra displayed as expected a single AX pattern that is distinguished by a large splitting due to ¹J_{PP} (see Table 4 for data). Studies on representative samples indicated that the chemical shifts exhibit some solvent dependence (e.g., both signals of **4b** displayed in acetonitrile by 4–6 ppm larger chemical shifts than in toluene), which is, however, much smaller than in *N*-heterocyclic *P*-chlorophosphines.²⁴ A comprehensive investigation of solvent effects was precluded by the high sensitivity of some substrates and their reactivity toward polar solvents.^{11a} The spectra of solid **4a–c, e, g** consist accord-

Table 2. Selected Bond Distances (Å) and Angular Parameters (deg) for **4a–f**

	R ^{1a}	R ²	P–P	P–P(2)–C	Σ∠(P2) ^b	β ₁ ^c	P–P(1)–N	β ₂ ^d	Δ _p ^e	φ ^f
4a ^{g,h}	Mes	H	2.484(1)	81.9(1) 81.1(1)	253.5(3)	76	110.9(1) 109.7(1)	115	0.6	38
4b ^g	DIPP	H	2.409(1)	81.9(1) 84.8(1)	257.0(3)	80	105.4(1) 114.9(1)	114	0.4	33
4c ^g	Mes	Me	2.701(2)	79.4(2) 78.6(2)	248.5(6)	72	113.9(2) 117.0(2)	125	0.8	53
4d ⁱ	Mes	H	2.356(1)	88.0(1) 88.9(1)	267.0(3)	88	103.3(1) 103.7(1)	101	0.1	11
4e ^j	DMP	H	2.437(1)	86.9(1) 86.8(1)	264.6(3)	85	108.5(1) 105.2(1)	110	0.2	25
4f ^g	#1 ^k	DIPP	2.521(1)	83.7(1) 87.3(1)	261.5(3)	83	112.2(1) 116.2(1)	127	0.3	45
	#2 ^k		2.565(1)	80.9(1) 81.2(1)	253.0(3)	76	113.2(1) 117.4(1)	128	0.6	53

^a Mes = 2,4,6-trimethylphenyl, DMP = 2,6-dimethylphenyl, DIPP = 2,6-diisopropylphenyl. ^b Sum of bond angles around P2. ^c Angle between the phosphole plane and the P–P bond. ^d Angle between the diazaphospholene ring plane and the P–P bond. ^e Distance between the phosphole P atom and the projection of the diazaphospholene P atom on the phosphole plane. ^f Interplanar angle (deg) between the planes of the diazaphospholene and phosphole rings. ^g 2,3,4,5-Tetraethyl substituted phospholyl group. ^h Data from ref 11a (CCDC-232848). ⁱ 3,4-dimethyl substituted phospholyl group; ^j 2,4-Dimethyl-3,5-diphenyl substituted phospholyl group. ^k Two crystallographically independent molecules.

**Figure 3.** Overlay of the cyclic cores of **4a**, **4c**, and **4d**. The molecular structures are arranged in a way that the phosphole rings are superimposed on each other.**Chart 3****Table 3.** P–P Distances (Å) and P–P–C(N) Valence Angles (deg) for **7** after Energy Optimization of the Molecular Structure at Different Levels of Theory

	P–P	C–P(2)–P(1)	N–P(1)–P(2)
B3LYP/6-31 g(d)	2.528	85.4	104.4
B3LYP/6-311 g(d,p)	2.521	84.1	104.8
B3LYP/cc-pVDZ	2.563	84.3	104.6
B3LYP/cc-pVTZ	2.528	85.4	104.4
MP2/6-31 g(d)	2.693	87.6	102.8
MP2/cc-pVDZ	2.707	73.5	107.0
MP4(SDQ)/6-31 g(d)	2.418	87.5	102.8
CC(D)/6-31 g(d)	2.414	87.6	102.8
CC(D)/cc-pVDZ	2.463	85.3	102.7
CC(SD)/6-31 g(d)	2.408	88.1	102.7

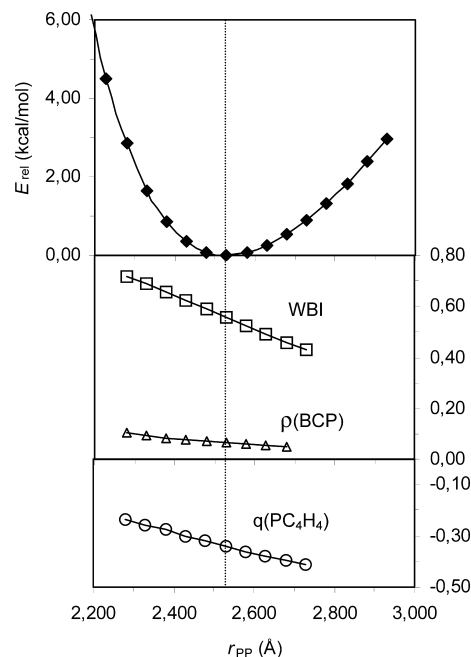
ingly of two spinning sideband manifolds that differ significantly in their shielding anisotropies and each represent the resonance of one type of phosphorus atom. The signals of ³¹P nuclei in the phosphole moiety appear, as in solution, as doublets with a splitting of ¹J_{PP}, whereas the signals of *N*-substituted phosphorus atoms are unresolved multiplets due to superposition of the homonuclear coupling with splittings arising from residual dipolar interactions with the adjacent ¹⁴N (*I* = 1) nuclei. The presence of the homonuclear coupling is nonetheless confirmed by measurement of *J*-resolved 2D-NMR spectra, which also allow precise determination of the magnitude of ¹J_{PP} in the indirect domain. Values of isotropic chemical shifts δ_{iso,solid} and the coupling constant ¹J_{PP,solid} are listed in Table 4.

Table 4. ³¹P Chemical Shifts and ¹J_{PP} Couplings in Solid-State and Solution NMR Spectra of **4a–g**

	solution			solid state		
	δ _{soln} (N ₂ P)	δ _{soln} (PC ₂)	¹ J _{PP,soln} [Hz] ^b	δ _{iso,solid} (N ₂ P)	δ _{iso,solid} (PC ₂)	¹ J _{PP,solid} [Hz] ^b
4a	147.1	23.1	188	147.8	31.2	161
4b	153.2	27.6	239	142.2	16.9	222
4c	170.9	47.5	134	171.9	49.8	73
4d	#1 ^a	135.7	5.2	128.1	−3.5	221
	#2 ^a			196	134.0	3.5
4e	148.7	36.6	190	142.8	29.9	198
4f	#1 ^a	170.8	51.8	185.2	42.0	−216
	#2 ^a			189.2	46.4	−160
4g	146.9	22.5	189	142.7	29.6	196

^a Distinguishable molecules in the solid state. ^b Absolute values unless indicated otherwise.

Solid **4f** contains two crystallographically independent molecules that give rise to distinguishable NMR signals, and the ³¹P CP-MAS NMR spectrum consists accordingly of two pairs of sideband manifolds of equal overall intensity. As signal duplication is also observed for **4d**, we presume that the material

**Figure 4.** Calculated energies (♦ top), P–P WBI bond index (□), electron densities at the P–P bond critical point (Δ), and sums of NBO charges of the atoms in the phosphole moiety (○) of **7** during a relaxed potential energy scan involving stepwise variation of the P–P distance. All calculations were carried out at the B3LYP/6-31g(d,p)//B3LYP/6-31g(d) level.

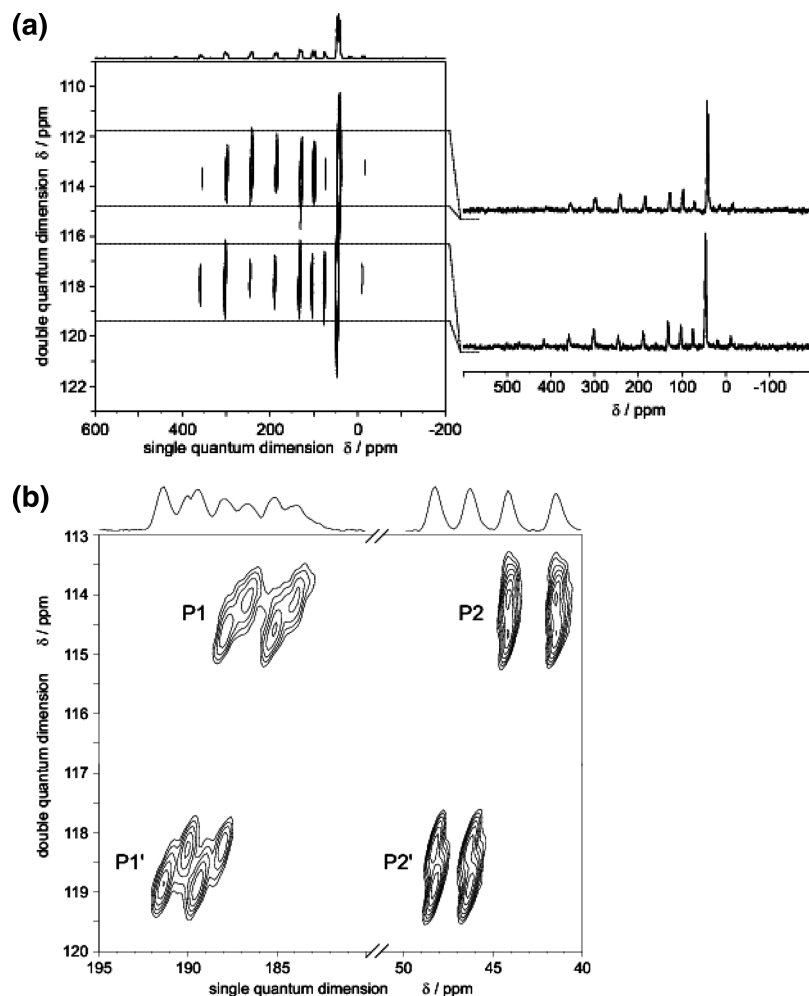


Figure 5. (a) ^{31}P CP MAS 2D single-quantum double-quantum correlation NMR spectrum of **4f** (MAS frequency 4.6 kHz, resonance frequency 81.0 MHz, C9_1^4 with a Postelement²⁶) showing the resolution of the overlapping spinning sideband patterns of both crystallographically independent molecules. The principal axes values for the P-atoms in the diazaphospholene ring were estimated from the sum projections shown on the right-hand side (see Supporting Information). (b) ^{31}P CP-MAS INADEQUATE NMR spectrum of **4f** (MAS frequency 25 kHz, 2.8 ms double-quantum conversion period, 81.0 MHz resonance frequency) resolving the four multiplets from the two different molecules **4f#1**, **4f#2** in the crystal. The doublet patterns in the direct dimension arise from the $^1J_{\text{PP}}$ coupling and the complicated splittings (approximately 4:4:1) in the indirect dimension from the coupling to two ^{14}N atoms in the diazaphospholene ring.

submitted to the NMR measurement is a polymorph of the sample characterized by single-crystal X-ray diffraction, which contains likewise two crystallographically independent molecules per unit cell. Signals of mutually coupled nuclei belonging to one molecule of **4d** or **4f** were identified from 2D-NMR spectra (J -resolved or INADEQUATE, Figure 5a), and the results are included in Table 4.

To enable detailed understanding of the connection between structural changes and NMR data, it is desirable to assign the observed signals to the two entities **4f#1** and **4f#2** present in crystalline **4f**. To this end, we determined J -couplings, ^{31}P chemical shift tensors, and effective magnetic dipole–dipole coupling constants from the experimental spectra and compared the results with calculated values obtained from computational studies. Full resolution and assignment of the spinning sideband patterns of both independent molecules was feasible with the help of a 2D double-quantum single-quantum correlation experiment (C9_1^4 with a Postelement,²⁶ Figure 5a) and 2D-

INADEQUATE (Figure 5b), which shows the typical pattern²⁷ caused by ^{14}N – ^{31}P quadrupolar-dipolar cross-terms from two ^{14}N atoms with a quadrupole coupling constant of approximately 4 MHz. The 2D experiment using C9_1^4 allows solution of the spinning sideband patterns for **4f#1** and **4f#2** since it can be used at slow-spinning speeds.²⁶ Simulation of the resolved traces made it possible to determine the principal axes values of the ^{31}P chemical shift tensors for the P-atoms in the N -heterocyclic rings of both specimen. Comparison of experimental anisotropic chemical shifts with predicted ones obtained from quantum mechanical calculations permitted a first assignment of the signals to **4f#1** and **4f#2** (see Supporting Information). Moreover, the simulation allowed unambiguous determination of the sign of $^1J_{\text{PP}}$ ²⁸ based on “roof effects” in the J -coupling multiplets (Supporting Information). For both molecules, the

(27) Hughes, C. E.; Pratima, R.; Karlsson, T.; Levitt, M. H. *J. Magn. Reson.* **2002**, *159*, 25.

(28) Wu, G.; Sun, B.; Wasylishen, R. E.; Griffin, R. G. *J. Magn. Reson.* **1997**, *124*, 366.

(26) Schmedt auf der Günne, J. *J. Magn. Reson.* **2003**, *165*, 18.

Table 5. DFT-Calculated $^1J_{PP}$ Coupling Tensors for **7** (All Data in Hz)^a

	7#1	7#2
Fermi contact (FC)	-218.7	-130.1
paramagnetic spin-orbital (PSO)	-3.4	-3.7
diamagnetic spin-orbital (PSO)	0.3	0.3
spin-dipole (SD)	-3.0	-5.1
total $J_{iso,calc}$	-221.8	-133.5
$\Delta J = J_{ } - J_{\perp}$ ^b	-168	-145
$D^{eff,calc} = D - \Delta J/3$ ^c	-1190	-1121
J_{exp}	-216	-160
$D^{eff,exp}$	-1196	-1097

^a B3LYP results with IGLO-III basis on P and IGLO-II on the other atoms, see Computational Details. ^b Obtained by transformation of the J -tensor to the coordinate frame of the D -tensor. ^c D was computed using the P–P distance measured in the crystal structure.

isotropic J -coupling constant is negative, in accord with previous findings on the sign of this coupling in phosphine derivatives.²⁹

If one recalls, however, that **4f#1** and **4f#2** exhibit a perceptible difference in P–P distances r_{PP} , they should likewise display noticeably different dipolar coupling constants $D_{PP} = -(\mu_0\hbar/8\pi^2)(\gamma_P)^2/(r_{PP})^3$ (in Hz), and measurement of D_{PP} should thus confirm the solution to the assignment problem. A viable approach to solve this task is the double quantum dephasing (DoDe) experiment,²⁹ which allows evaluation of effective dipolar coupling constants $D^{eff}_{AB} = D_{AB} - \Delta J_{AB}/3$, where D_{AB} denotes the direct dipolar coupling and ΔJ_{AB} the anisotropy of the scalar coupling tensor, in homonuclear spin pairs under magic angle spinning. Performing this experiment on **4f** made it possible to determine values of $D^{eff} = -1196$ Hz for the doublet at $\delta^{31P} = 42.0$ with $^1J_{PP} = -217$ Hz and $D^{eff} = -1097$ Hz for the doublet at $\delta^{31P} = 46.4$ with $^1J_{PP} = -160$ Hz, respectively. These values compare well with dipolar couplings calculated from observed distances ($D = -1246$ Hz (**4f#1**), -1169 Hz (**4f#2**)).

In view of the difficulties associated with experimental determination of ΔJ ,³¹ we decided to assess its magnitude by quantum-chemical computation of the coupling tensor for the model diphosphine **7**. Calculations were carried out for two specimen **7#1** and **7#2** whose molecular structures are based on the crystallographic coordinates of **4f#1** and **4f#2**. Results are listed together with the experimental values of $^1J_{PP}$ and D^{eff} in Table 5. The excellent agreement between calculated and experimental values of both isotropic couplings $^1J_{PP}$ and effective dipolar couplings D^{eff} is immediately evident and eliminates any remaining ambiguities in the given spectral assignment that might be associated with the influence of ΔJ . According to the model calculations on **7**, $^1J_{PP}$ is clearly dominated by the Fermi-contact term, whose magnitude varies with internuclear distance. It therefore appears straightforward to connect the overall variance of $^1J_{PP,solid}$ in **4a–g** (Table 4) with the change in r_{PP} . This hypothesis is indeed supported by the observed relation (Figure 6).

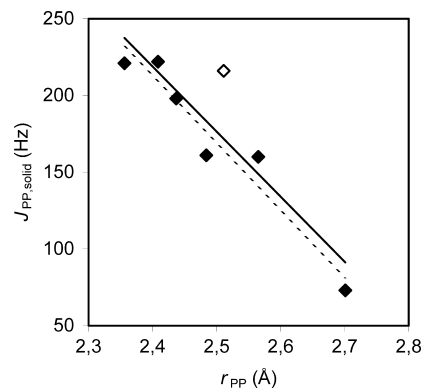


Figure 6. Plot of $^1J_{PP,solid}$ versus r_{PP} for **4a–f**. Straight lines denote results of linear correlation analyses (solid line = all data, $R^2 = 0.81$; dashed line = **4f#1** excluded as outlier, $R^2 = 0.94$).

Direct comparison of solution and solid-state 31P NMR data of **4a–g** reveals minor deviations between isotropic chemical shifts in solution (δ_{soln}) and solid state ($\delta_{iso,solid}$), which are common for phosphine derivatives and are attributed to unspecific solvation influences. In contrast, the coupling constants display quite large differences that may even exceed 100 Hz in magnitude (cf. Table 4), and a plot of $^1J_{PP,soln}$ versus $^1J_{PP,solid}$ (see Supporting Information) reveals that trends in both quantities appear to be unrelated. As scalar couplings are exclusively determined by intramolecular factors, these deviations suggest the presence of perceptible differences between solid-state and solution structures of **4a–g**.

Recalling that the crystal structure data of **4a–f** suggest P–P distances and phosphorus valence angles as most easily distorted internal coordinates, we decided to evaluate the influence of changes in these parameters on $^1J_{PP}$ by computational studies on the model compound **7**. In addition, we considered also the influence of internal rotation around the P–P bond (represented by a torsional angle θ between the planes intersecting the N–P(1)–N and C–P(2)–C valence angles), which is known to have a strong influence on $^1J_{PP}$ ^{29,32} and, although not of importance in solid **4a–f**, might occur in solution. As a means for testing, we carried out relaxed potential energy (PE) scans by incrementing r_{PP} or θ and reoptimizing the other internal coordinates (due to the correlation between changes in r_{PP} , phosphorus valence angles, and the interplanar angle ϕ , additional PE scans with variation of these angular coordinates were considered unnecessary), and calculated $^1J_{PP}$ at each point. Graphical analysis of the results of a PE scan performed by incrementing r_{PP} (Figure 7) revealed that larger internuclear distances coincide with a numerical increase (i.e., a decrease in magnitude) in $^1J_{PP}$ which reproduces the experimentally observed relation between both parameters. An interesting aspect is that at larger distances $^1J_{PP}$ approaches not zero asymptotically but changes its sign. However, studies at more elaborate theoretical levels are certainly required to establish if this effect is real or merely an artifact of the computational model.

Analysis of the dependence of $^1J_{PP}$ on the torsional angle θ was more complicated as variation of θ was connected with simultaneous relaxation of r_{PP} . The changes in both $^1J_{PP}$ and r_{PP} with θ showed very similar patterns (Figure 8), and linear

(29) (a) Jameson, C. J. In *Phosphorus-31 NMR Spectroscopy in Stereochemical Analysis*; Verkade, J. G., Quin, L. D., Eds.; VCH Publishers: Deerfield Beach, 1987; p 205 ff. (b) Verkade, J. G.; Mosbo, J. A. In *Phosphorus-31 NMR Spectroscopy in Stereochemical Analysis*; Verkade, J. G., Quin, L. D., Eds.; VCH Publishers: Deerfield Beach, 1987; 425 ff and cited references.

(30) Schmedt auf der Gönne, J. J. *Magn. Reson.* **2006**, *180*, 186.

(31) (a) Grimmer, A. R.; Peter, R.; Fechner, E. *Z. Chem.* **1978**, *18*, 109. (b) Nakai, T.; McDowell, C. A. *J. Am. Chem. Soc.* **1994**, *116*, 6373. (c) Gee, M.; Wasylischen, R. E.; Ragogna, P. J.; Burford, N.; McDonald, R. *Can. J. Chem.* **2002**, *80*, 1488.

(32) (a) Duangthai, S.; Webb, G. A. *Org. Magn. Reson.* **1983**, *21*, 199. (b) Galasso, V. J. *Magn. Reson.* **1979**, *36*, 181. (c) Albrand, J. P.; Faucher, H.; Gagnaire, D.; Robert, J. B. *Chem. Phys. Lett.* **1976**, *38*, 521. (d) Cowley, A. H.; White, W. D. *J. Am. Chem. Soc.* **1969**, *91*, 1917.

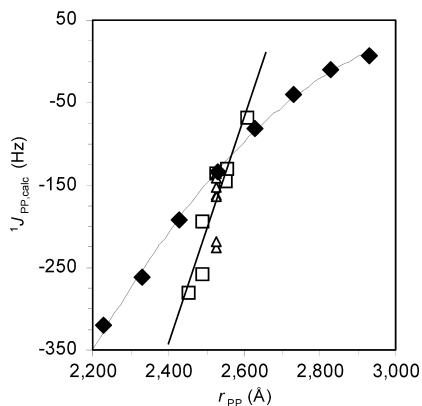


Figure 7. Plot of $^1J_{PP,calc}$ versus r_{PP} during PE scans of **7**. Diamonds (◆) denote values of $^1J_{PP,calc}$ for a relaxed PE scan with variation of r_{PP} that did not cause any deviation of θ from 0° (correlation analysis gave $J_{PP,calc} = -408r_{PP}^2 + 2588r_{PP} - 4070$, $R^2 = 0.998$). Squares (□) refer to a relaxed PE scan under variation of θ (correlation analysis gave $J_{PP,calc} = 1393r_{PP} - 3689$, $R^2 = 0.91$). Triangles (Δ) refer to a PE scan under variation of θ with r_{PP} remaining fixed to its equilibrium value (2.528 Å).

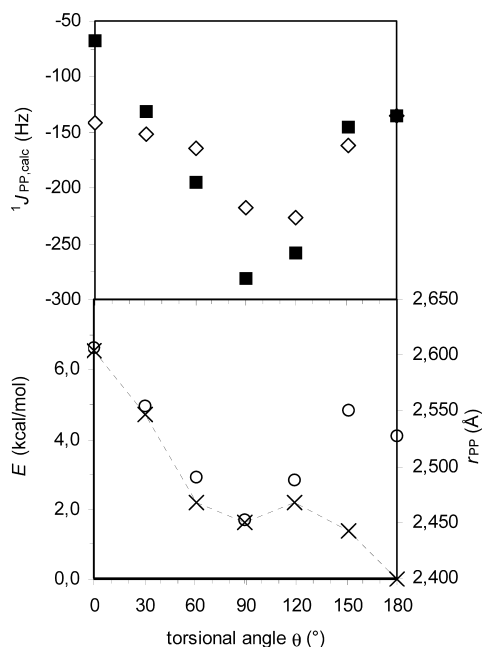


Figure 8. Variation of $^1J_{PP,calc}$, total energy E (×), and r_{PP} (○) of **7** during PE scans under variation of θ . Squares (■) denote values of $^1J_{PP,calc}$ for a fully relaxed PE scans under variation of r_{PP} , and diamonds (◆) refer to variation of θ with r_{PP} fixed to its equilibrium value (2.528 Å).

regression between $^1J_{PP}$ and values of $r_{PP}(\theta)$ associated with different torsional angles θ gave in fact a reasonable correlation (Figure 7). However, as variation of *both* r_{PP} and θ exerts a clearly larger effect on $^1J_{PP}$ (judging by the slopes of the correlation lines in Figure 7) than a change in r_{PP} alone, it is unlikely that the dependence of $^1J_{PP}$ on θ owes exclusively to the change in internuclear distance. In fact, performing a partially relaxed PE scan with variation of θ under the constraint that r_{PP} was fixed to its equilibrium value confirmed earlier experimental and theoretical findings^{32,29} of a marked direct dependence of $^1J_{PP}$ on the torsion angle θ (Figure 8); however, as those conformers with nearly orthogonal phosphorus lone pairs ($\theta \approx 90\text{--}120^\circ$) that give the largest couplings (in terms of absolute value)²⁹ exhibit also the shortest bonds, the contributions of changes in r_{PP} and θ on $^1J_{PP}$ follow nearly parallel trends, and their independent evaluation is unfeasible.

The calculated bond torsion energy profiles (Figure 8) suggest further the existence of a second rotamer with *gauche* arrangement of both five-membered rings and slightly higher energy than the *trans* conformer, which was successfully located in a subsequent full energy optimization. Harmonic frequency calculations allowed to identify both the *trans* ($\theta = 180^\circ$) and *gauche* rotamer ($\theta = 89.4^\circ$) as local minima on the PE surface and the conformer at highest energy ($\theta = 0^\circ$) as transition state.

The results of computational and experimental studies attesting the influence of geometric distortions in **4f#1** and **4f#2** on $^1J_{PP}$ suggest that deviations between $^1J_{PP,solid}$ and $^1J_{PP,soln}$ in one compound are attributable to two possible sources, viz., (a) occurrence of different P–P bond lengths in solution and solid state or (b) presence of a major amount of *gauche* rotamers in solution beside (or instead of) the *trans* rotamers found in the solid state. Solvent induced changes in bond lengths had previously been suggested for *N*-heterocyclic *P*-chlorophosphines.^{24,25} Predominance of a *gauche* isomer in the solid state and at low temperature in solution had been proven for a Cp*-substituted derivative,³³ and equilibria between different rotamers are well established for diphosphine derivatives.²⁹

Low-temperature NMR studies of diphosphines **4** gave no evidence for temperature-dependent line shape changes³³ that might allow positive identification of *gauche* rotamers in solution and supported thus the previously derived assignment of the *trans* rotamers as most stable conformers. On the other hand, these experiments disclosed also a pronounced increase in $^1J_{PP}$ with temperature,³⁴ which is known to indicate shifts in the relative populations of different rotamers.²⁹ On the basis of the computed torsional energy profile of **7**, the observed behavior of the real molecules **4** is readily explained by postulating that the solutions contain a rapidly exchanging equilibrium mixture of *gauche* and *trans* rotamers with a growing population of the energetically less favorable *gauche* isomer at higher temperatures. However, if one considers that $^1J_{PP,solid}$ must in the absence of any change in r_{PP} be considered as lower boundary for $^1J_{PP,soln}$ (as $^1J_{PP,trans} < ^1J_{PP,gauche}$, any contribution by the *gauche* isomer in solution must inevitably result in a larger coupling size) and that this condition is obviously violated in some compounds (cf. Table 4; another example is **4b**, which obeys the condition at room temperature where $^1J_{PP,soln} = 239\text{ Hz} > ^1J_{PP,solid} = 222\text{ Hz}$ but not at 198 K where $^1J_{PP,soln} = 213\text{ Hz} < ^1J_{PP,solid} = 222\text{ Hz}$), we conclude that the deviations in $^1J_{PP}$ between solution and solid state are caused by a combination of the influences of the temperature-dependent conformer equilibrium on $^1J_{PP,soln}$ and some solvation-induced change in P–P bond lengths (aside from the intrinsic shortening of r_{PP} in *gauche* conformers). It should be noted that this analysis is at present purely qualitative in character and allows neither the exclusion of contributions of further structural changes (e.g., in bond angles) nor quantitative assessment of conformer ratios or individual bond length variations; however, the observation of a reduced magnitude of $^1J_{PP,soln}$ as compared to $^1J_{PP,solid}$ in some compounds provides a strong argument to postulate that the solution structures feature in these cases still longer P–P bonds than the crystalline samples.

(33) Burck, S.; Gudat, D.; Nieger, M.; Tirr e, J. *Dalton Trans.* **2007**, 1891.

(34) For example, $^1J_{PP}$ of **4a** showed a temperature-dependent variation from 177 Hz (198 K) to 191 Hz (303 K), which could be fitted to a second order polynomial ($J(T) = 7 \times 10^{-4} T^2 - 0.227T + 194.1$, $R^2 = 0.997$); similarly, $^1J_{PP}$ of **4b** varied from 213 Hz (198 K) to 271 Hz (363 K), obeying the equation ($J(T) = 1 \times 10^{-3} T^2 - 0.182T + 211.0$, $R^2 = 0.998$).

Discussion of the Bonding Situation in Polarized Diphosphines. Summarizing the most prominent results derived from the X-ray diffraction studies makes it possible to state that the diphosphines **4** exhibit P–P bonds that are generally much longer than normal single bonds, display a unique flexibility as subtle changes in peripheral *N*-aryl substituents may induce bond length distortions over a range of more than 0.15 Å, and respond sensitively to the presence of substituents capable of inductive stabilization of the π -electron system in the *N*-heterocyclic ring. All of these features represent typical attributes of molecular systems containing a dative (donor–acceptor) bond according to the definition by R. S. Mulliken³ or A. Haaland.⁴ That the P–P bonds display also a substantial polarity and the tendency to undergo heterolytic rather than homolytic cleavage, which are further essentials of dative bonds,⁴ is strongly supported by (a) natural population analyses for the model compound **7** that indicate the buildup of considerable partial charges on phospholyl and diazaphospholenyl fragments ($q = \pm 0.34$ at the B3LYP/6-31 g(d) level and the optimized molecular geometry) that increases upon further bond lengthening (Figure 4) and (b) the observed thermal³⁵ and chemical behavior^{11,12} of **4** that is best rationalized by describing these molecules as consisting of a nucleophilic phospholyl and an electrophilic phosphonium fragment. The P–P bond polarity suggests a marked electrostatic bonding contribution that is offset by a decrease in covalent bond order (cf. a remarkably small Wiberg bond index of 0.55 at the equilibrium geometry, which decreases upon further bond lengthening, Figure 4). This intermediate bonding situation (between genuine covalent and ionic) is also highlighted by a topological analysis of the electron density,³⁶ which reveals that the electron density at the bond critical point is generally low (Figure 4) and the Laplacian changes with increasing bond lengthening from small negative to small positive values (see Supporting Information). The topological analysis discloses further that the structural distortion, which is represented by the move of the diazaphospholene ring from a peripheral position toward the centroid of the phosphole ring and the concomitant bond lengthening (Figure 3, Table 4), does not produce new bond or cage critical points; this suggests that the covalent interaction remains localized between the phosphorus atoms and should not be interpreted in terms of π -bonding between the phosphole and diazaphospholene units. The geometrical distortion is thus best explained as a consequence of increasing ionicity, which favors a closer approach of the positively charged phosphonium fragment to the center of the negative charge in the phosphole π -system. This view is also in accord with the low degree of π -delocalization in the phosphole, which is incompatible with a description of a truly aromatic ring. On the whole, all aspects suggest a picture of the bonding situation in the diphosphines **4** in a similar manner as in *N*-heterocyclic *P*-chlorophosphines^{20,24,25} as hybrid between a covalent molecule and a phosphonium-phospholide contact ion pair (albeit with a somewhat lower ionic contribution), with a P–P bond that is best described as dative

donor–acceptor interaction (or a highly polarized covalent bond) rather than a “normal”⁴ covalent bond.

Conclusions

The results of structural, spectroscopic, and computational studies on a series of *P*-phospholyl-diazaphospholenes **4** reveal that the unusually long P–P bonds exhibit specific features of dative bonds in the sense of Haaland⁴ that are regarded to result from donor–acceptor interaction between a Lewis acid/base pair rather than combination of two radicals. These findings suggest classification of compounds **4** as hybrids between phosphonium-phospholide donor–acceptor complexes and genuine covalent molecules, which is in accord with their capability to undergo reactions under heterolytic P–P bond cleavage.^{11,12} Analysis of trends in $^1J_{PP}$ coupling constants in the solid state and solution established an inverse relation between the magnitude of $^1J_{PP, \text{solid}}$ and the P–P bond distance and indicated that the large deviations between $^1J_{PP, \text{soln}}$ and $^1J_{PP, \text{solid}}$ and the temperature dependence of the former are caused by an equilibrium between *trans* and *gauche* rotamers in solution in combination with solvation-induced relaxation of bond lengths. The observation of this effect, which had previously been discussed for *N*-heterocyclic *P*-chlorophosphines,^{24,25} can be regarded as further argument to support the view of the P–P bond as donor–acceptor interaction. The distance dependence of $^1J_{PP}$ is in line with the dominance of the Fermi contact contribution to the coupling and is presumably also of importance for all other diphosphine derivatives where the same situation applies. Critical evaluation of the results of the solid-state ^{31}P NMR studies substantiates further that splittings caused by quadrupolar-dipolar ^{31}P – ^{14}N cross-terms can significantly broaden ^{31}P NMR signals and that the anisotropy of $^1J_{PP}$ -coupling may limit the accuracy of P–P distance termination by solid-state NMR experiments to 10 pm.

Experimental Section

All manipulations were carried out under an atmosphere of dry argon using standard vacuum line techniques. Solvents were dried by standard procedures. EI-MS: Varian MAT 711, 70 eV. Elemental analysis: Perkin-Elmer 2400CHN/O Analyzer. Melting points were determined in sealed capillaries.

Solution NMR spectra were recorded on Bruker Avance 400 (^1H , 400.1 MHz; ^{13}C , 100.5 MHz; ^{31}P , 161.9 MHz) or Avance 250 (^1H , 250.1 MHz; ^{13}C , 62.8 MHz; ^{31}P , 101.2 MHz) NMR spectrometers at 303 K. 1D Solid-state ^{31}P NMR spectra were acquired on a Bruker Avance 400 spectrometer (^1H , 400.1 MHz; ^{31}P , 161.9 MHz) in 4 mm zirconia rotors under CP-MAS conditions using spin rates between 3.1 and 15 kHz that were carefully adjusted to avoid rotational resonance conditions. Spectra of all samples were recorded at several different spin rates, and it was verified that the positions and linewidths of all isotropic lines were independent of the spin rate. Multidimensional solid-state NMR experiments and DoDe experiments were recorded on a Bruker Avance II 200 spectrometer (^1H , 200.1 MHz; ^{31}P : 81.1 MHz) with a double-resonance MAS probe and zirconia rotors with 2.5 mm outer diameter. All experiments used continuous wave ^1H decoupling at 160 kHz for periods during which multipulse sequences were used on ^{31}P , and 100 kHz during periods of free evolution. Contact times of 5 ms were used for cross-polarization. 2D correlation spectra used rotor synchronized sampling for the indirect dimension. Double-quantum dephasing experiments (DoDe)³⁰ were conducted at 8 kHz sample-spinning frequency. An INADEQUATE sequence prepared double-quantum coherence in 2.8 ms, dephasing was

(35) No evidence for radical formation that had been observed in other cases (e.g., ref 6; see also Bezombes, P. J.; Hitchcock, P. B.; Lappert, M. F.; Nycz, J. E. *Dalton Trans.* **2004**, 499.) was observable for **4a**–**g** up to 100°C.

(36) (a) Bader, R. F. W.; Nguyen-Dang, T. T.; Tal, Y. *Rep. Prog. Phys.* **1981**, *44*, 895. (b) Bader, R. F. W. *Atoms in Molecules: A Quantum Theory*; Clarendon Press: Oxford, 1990.

achieved with POSTC7,³⁷ and reconversion was realized again with an INADEQUATE sequence preparing double-quantum coherence in 2.8 ms. The reported effective dipole coupling constants are average values from five experiments with different dephasing periods (τ_{total} between 3 and 5 ms) and exhibit a standard deviation of approximately 37 Hz. For the analysis of the DoDe values it was necessary to include the chemical shift tensors into the fit procedure³⁸ because PostC7 under the chosen conditions does not fully suppress the influence of the chemical shift. Chemical shifts are referenced to ext. TMS (¹H, ¹³C) or 85% H₃PO₄ ($\Xi = 40.480747$ MHz, ³¹P), and coupling constants are given as absolute values if not indicated otherwise; *i*, *o*, *m*, *p* denote the positions in *N*-aryl rings.

Computational studies aimed at exploring the potential energy hypersurface of **7** and the influence of geometrical changes on ¹J_{PP} were performed with the Gaussian 03³⁹ program suite. DFT calculations were generally carried out using Becke's 3-parameter exchange functional⁴⁰ with the Lee–Yang–Parr correlation energy functional (B3LYP)⁴¹ with 6-31g(d) basis sets for geometry optimization and 6-31g(d,p) basis sets for the computation of coupling constants. Numerical integrations were performed on an ultrafine grid. Harmonic frequencies and zero-point energies (ZPE) at optimized gas-phase structures were calculated at the same level and served to identify local minima (only positive eigenvalues of the Hessian matrix) or transition states (one negative eigenvalue) on the potential energy surface. Further structure optimizations were carried out at higher theoretical levels as specified in Table 3. Natural population analyses⁴² were carried out with the NBO module in Gaussian03. Listings of atomic coordinates and absolute energies are given as Supporting Information. Evaluation of the electron density at bond critical points was performed with the program MORPHY.⁴³

Additional calculations of the spin–spin coupling tensors were done with the combined analytical/finite perturbation approach of ref 44, as implemented in the MAG-ReSpect program package.⁴⁵ Kohn–Sham molecular orbitals obtained with Gaussian 03, the B3LYP functional, IGLO-III basis set⁴⁶ for phosphorus, and IGLO-II basis sets⁴⁶ for the other atoms were transferred to the MAG module by suitable interface routines. A finite perturbation parameter of $\lambda = 10^{-3}$ au was used for the Fermi contact perturbation in Gaussian 03. In addition to the FC contribution to the isotropic coupling, this procedure provides also the FC/SD cross term that dominates *J*_{aniso}. From the general axes system of the molecular framework, the *J*-tensor was subsequently transformed to an axis system in which the P–P bond corresponds to the *z*-axis (large “parallel component” of *J*-anisotropy), and the larger of the two perpendicular components (*J*_{yy}) is in the P2–P1–N1 plane. This orientation is consistent with that of the full measured anisotropic

coupling tensor and thus allowed us to obtain the pure dipolar contribution by subtraction of the computed *J*-anisotropy from the full coupling anisotropy. The SD contribution to the coupling, which is not contained in the output of the MAG-ReSpect program, was computed in Gaussian03 using the same basis set.

1-Chloro-3,5-dimethyl-2,4-diphenylphosphole 6. Butyllithium (120 mmol, 48 mL of 2.5 M solution in hexane) was slowly added to a cooled (–78 °C) solution of zirconocene dichloride (17.53 g, 60 mmol) and 1-phenylpropyne (13.92 g, 120 mmol) in THF (80 mL). The mixture was stirred for 0.5 h at –78 °C and then allowed to warm to room temperature. The solvent was removed in vacuum, and the residue dissolved in toluene (50 mL). The filtrate was evaporated to dryness, and the residue was redissolved in THF (50 mL). The solution was cooled to –78 °C, and phosphorus trichloride (8.25 g, 60 mmol) was slowly added. The mixture was then allowed to warm to room temperature and stirred for 18 h. Solvents were then removed in a vacuum, and the residue was extracted with hexane (100 mL). Precipitated salts were removed by filtration, the solvent was evaporated in a vacuum, and the residue was subjected to fractionate distillation in vacuum. The product was obtained as yellow oil, bp 82 °C/10^{–3} mbar, which solidified on standing (yield 12.97 g, 73%, mp 25 °C). ¹H NMR (CD₃CN) δ 7.52–7.11 (m, 10 H, H_{phenyl}), 2.01 (d, 3 H, ³J_{PH} = 11.2 Hz, CH₃), 1.87 (d, 3 H, ⁴J_{PH} = 5.9 Hz, CH₃); ³¹P{¹H} NMR (CD₃CN) δ 78.7 (s).

Preparation of 2-(2',3',4',5'-Tetraethylphospholy)-dihydro-1,3,2-diazaphospholes 4b,c,f,g. Lithium (10 mmol) was added to a solution of 1-chloro-2,3,4,5-tetraethylphosphole (5 mmol) in THF (20 mL). The mixture was stirred for 3 h at room temperature before unreacted metal was removed by filtration. The remaining solution was slowly added to a cooled (–78 °C) solution of the appropriate 2-chloro-dihydro-1,3,2-diazaphosphole (5 mmol) in THF (50 mL). The solution was then allowed to warm to room temperature and stirred for 1 h at this temperature. Solvent was then removed under reduced pressure, and the residue was treated with hexane (50 mL). The formed suspension was filtered over Celite, and the filtrate evaporated to dryness. The crude product was purified by recrystallization from appropriate solvents.

4b: recrystallization from hexane at –20 °C, yield 2.65 g (88%), mp 92 °C; ¹H NMR (C₆D₆) δ 7.21–7.07 (m, 6 H, *m/p*-H), 6.18 (d, 2 H, ³J_{PH} = 0.4 Hz, N–CH), 3.71 (sept, 2 H, ³J_{HH} = 6.7 Hz, CH), 3.70 (sept, 2 H, ³J_{HH} = 6.7 Hz, CH), 2.32 (q, 4 H, ³J_{HH} = 7.5 Hz, CH₂), 1.74 (m, 4 H, ³J_{HH} = 7.5 Hz, ³J_{PH} = 11.0 Hz, ⁴J_{PH} = 0.7 Hz, CH₂), 1.39 (d, 6 H, ³J_{HH} = 6.7 Hz, CH₃), 1.16 (d, 6 H, ³J_{HH} = 6.7 Hz, CH₃), 1.02 (t, 12 H, ³J_{HH} = 6.7 Hz, CH₃); ¹³C{¹H} NMR (C₆D₆) δ 151.9 (dd, *J*_{PC} = 7.3, 1.4 Hz, *i*-C), 147.0 (dd, *J*_{PC} = 3.1, 1.8 Hz, *o*-C), 142.7 (dd, ¹*J*_{PC} = 21.0 Hz, ²*J*_{PC} = 14.4 Hz, C_{phosphole}), 137.8 (dd, *J*_{PC} = 7.0, 1.4 Hz, C_{phosphole}), 127.8 (d, ⁵*J*_{PC} = 1.5 Hz, *p*-CH), 124.5 (d, ⁴*J*_{PC} = 0.5 Hz, *m*-CH), 122.3 (dd, *J*_{PC} = 9.2, 1.3 Hz, N–CH), 28.9 (dd, ⁴*J*_{PC} = 6.5 Hz, ⁵*J*_{PC} = 1.2 Hz, CH), 25.7 (s, CH₃), 23.3 (dd, ⁶*J*_{PC} = 2.0 Hz, ⁷*J*_{PC} = 2.0 Hz, CH₃), 21.2 (d, ³*J*_{PC} = 1.5 Hz, CH₂), 21.0 (dd, *J*_{PC} = 22.0, 1.4 Hz, CH₂), 18.7 (dd, ³*J*_{PC} = ⁴*J*_{PC} = 2.8 Hz, CH₃), 16.5 (d, ⁴*J*_{PC} = 1.2 Hz, CH₃); MS (EI, 70 eV, 370 K) *m/e* (%) 601.2 (0.1) [M]⁺, 407.2 (100) [M – C₁₂H₂₀P]⁺, 195.1 (40) [M – C₂₆H₃₆N₂P]⁺, C₃₈H₅₆N₂P₂ (602.82): C 75.71, H 9.36, N 4.65; found C 75.11, H 9.27, N 4.47.

4c: recrystallization from hexane/THF (10:1) at –20 °C, yield 2.39 g (88%), mp 132 °C; ¹H NMR (C₆D₆) δ 6.80 (s, 4 H, *m*-CH), 2.44 (q, 4 H, ³J_{HH} = 7.5 Hz, CH₂), 2.32 (s, 12 H, *o*-CH₃), 2.13 (s, 6 H, *p*-CH₃), 1.79 (m, 2 H, ³J_{HH} = 7.5 Hz, CH₂), 1.77 (m, 2 H, ³J_{HH} = 7.5 Hz, CH₂), 1.42 (s, 6 H, NCCH₃), 1.17 (t, 6 H, ³J_{HH} = 7.5 Hz, CH₃), 1.13 (t, 6 H, ³J_{HH} = 7.5 Hz, CH₃); ¹³C{¹H} NMR (C₆D₆) δ 149.7 (dd, *J*_{PC} = 10.9, 3.0 Hz, *i*-C), 144.3 (dd, ¹*J*_{PC} = 25.3 Hz, ²*J*_{PC} = 17.1 Hz, C_{phosphole}), 137.7 (dd, ³*J*_{PC} = 4.5 Hz, ⁴*J*_{PC} = 1.6 Hz, *o*-C), 137.6 (d, ⁵*J*_{PC} = 1.3 Hz, *p*-C), 135.2 (dd, *J*_{PC} = 7.1, 1.1 Hz, C_{phosphole}), 129.8 (s, *m*-CH), 124.8 (dd, *J*_{PC} = 8.6, 0.7 Hz, N–C), 21.6 (d, ²*J*_{PC} = 13.7 Hz, CH₂), 21.4 (d, ³*J*_{PC} = 8.4 Hz, CH₂), 21.1 (s, *o*-CH₃), 19.4 (d, ³*J*_{PC} = 1.4 Hz, CH₃), 19.3 (s, CH₃), 17.7 (s, *p*-CH₃), 11.4 (d, ³*J*_{PC} = 3.7 Hz, NC–CH₃); MS (EI, 70 eV, 400 K) *m/e* (%) 545.3 (0.1) [M – H]⁺, 351.1 (100) [M –

(37) Hohwy, M.; Jakobsen, H. J.; Edén, M.; Levitt, M. H.; Nielsen, N. C. *J. Chem. Phys.* **1998**, *108*, 2686.

(38) Bak, M.; Rasmussen, J. T.; Nielsen, N. C. *J. Magn. Reson.* **2000**, *147*, 296.

(39) Frisch, M. J. et al. *Gaussian 03, Revision E.01*; Gaussian Inc.: Pittsburgh, PA, 2003.

(40) Becke, A. D. *J. Chem. Phys.* **1993**, *98*, 5648.

(41) Lynch, B. J.; Fast, P. L.; Harris, M.; Truhlar, D. G. *J. Phys. Chem. A* **2000**, *104*, 4811.

(42) Reed, A. E.; Weinstock, R. B.; Weinhold, F. *J. Chem. Phys.* **1985**, *83*, 735.

(43) Popelier, P. L. A. *Comput. Phys. Commun.* **1996**, *93*, 212.

(44) (a) Malkin, V. G.; Malkina, O. L.; Eriksson, L. A.; Salahub, D. R., In *Modern Density Functional Theory: A Tool for Chemistry; Theoretical and Computational Chemistry*; Seminario, J. M., Politzer, P., Eds.; Elsevier: Amsterdam, 1995; Vol. 2. (b) Malkina, O. L.; Salahub, D. R.; Malkin, V. G. *J. Chem. Phys.* **1996**, *105*, 8793.

(45) Malkin, V. G.; Malkina, O. L.; Reviakine, R.; Arbuznikov, A. V.; Kaupp, M.; Schimmelpfennig, B.; Malkin, I.; Repický, M.; Komorovský, S.; Hrobarik, P.; Malkin, E.; Helgaker, T.; Ruud, K. *ReSpect, version 2.1*; 2006.

(46) Kutzelnigg, W.; Fleischer, U.; Schindler, M. In *NMR—Basic Principles and Progress*; Diehl, P., Fluck, E., Günther, H., Kosfeld, R., Eds.; Springer-Verlag: Heidelberg, Germany, 1990; Vol. 23, p 165.

$C_{12}H_{20}P]^+$, 196.1 (53) [$M - C_{26}H_{27}N_2P]^+$. $C_{34}H_{48}N_2P_2$ (546.72): C 74.70, H 8.85, N 5.12; found C 74.42, H 8.78, N 5.04.

4f: recrystallization from CH_3CN/THF (5:4) at -28 °C, yield 71%, mp 148 °C; 1H NMR (C_6D_6) δ 7.18 (m, 6 H, *m/p*-CH), 3.40 (sept, 4 H, $^3J_{HH} = 6.9$ Hz, CH), 2.50 (q, 4 H, $^3J_{HH} = 7.5$ Hz, CH_2), 1.98 (m, $^3J_{PH} = 11.4$ Hz, $^3J_{HH} = 7.5$ Hz, CH_2), 1.51 (s, 6 H, CH_3), 1.46 (d, 6 H, $^3J_{HH} = 7.5$ Hz, CH_3), 1.18 (d, 6 H, $^3J_{HH} = 7.5$ Hz, CH_3), 1.164 (t, 6 H, $^3J_{HH} = 7.5$ Hz, CH_3), 1.16 (t, 6 H, $^3J_{HH} = 7.5$ Hz, CH_3); $^{13}C\{^1H\}$ NMR (C_6D_6) δ 148.9 (dd, $^3J_{PC} = 4.2$ Hz, $^4J_{PC} = 2.1$ Hz, *o*-C), 147.1 (dd, $J_{PC} = 3.9$, 1.6 Hz, *i*-C), 140.9 (dd, $^1J_{PC} = 22.1$ Hz, $^2J_{PC} = 12.6$ Hz, $C_{phosphole}$), 135.5 (dd, $J_{PC} = 8.0$, 0.9 Hz, $C_{phosphol}$), 128.7 (d, $^5J_{PC} = 1.3$ Hz, *p*-CH), 124.8 (s, *m*-CH), 124.4 (dd, $J_{PC} = 8.8$, 1.7 Hz, *N*-C), 28.7 (dd, $^4J_{PC} = 2.6$ Hz, $^5J_{PC} = 1.3$ Hz, CH), 25.4 (dd, $^3J_{PC} = 5.7$ Hz, $^4J_{PC} = 2.0$ Hz, CH_2), 24.8 (s, CH_3), 21.0 (dd, $J_{PC} = 20.4$, 1.8 Hz, CH_2), 20.9 (d, $^4J_{PC} = 2.1$ Hz, CH_3), 19.3 (d, $^3J_{PC} = 3.9$ Hz, CH_3), 16.6 (s, CH_3), 12.3 (d, $^3J_{PC} = 2.9$ Hz, CH_3); MS (EI, 70 eV, 430 K) *m/e* (%) 470.1 (<0.1) [$M - C_{12}H_{16}]^+$, 452.4 (100) [$M - C_{12}H_{20}P+OH]^+$, 435.4 (84) [$M - C_{12}H_{20}P]^+$, 202.2 (84) [$M - C_{26}H_{40}NP_2]^+$, 194.1 (84) [$M - C_{28}H_{40}N_2P_2]^+$. $C_{40}H_{60}N_2P_2$ (630.88): C 76.14, H 9.59, N 4.44; found C 76.22, H 9.50, N 4.39.

4g: recrystallization from hexane/toluene (2:1) at -20 °C, yield 1.89 g (77%), mp 140 °C; 1H NMR (C_6D_6) δ 6.92 (s, 6 H, *m/p*-H), 5.80 (s, 2 H, *N*-CH), 2.32 (q, 4 H, $^3J_{HH} = 7.4$ Hz, CH_2), 2.44 (s, *o*- CH_3), 1.64 (q, 4 H, $^3J_{HH} = 7.4$ Hz, CH_2), 1.03 (t, 6 H, $^3J_{HH} = 7.4$ Hz, CH_3), 1.03 (t, 6 H, $^3J_{HH} = 7.4$ Hz, CH_3); $^{13}C\{^1H\}$ NMR (C_6D_6) δ 153.2 (dd, $J_{PC} = 8.9$, 2.6 Hz, 3/4-C), 144.0 (dd, $^1J_{PC} = 22.4$ Hz, $^2J_{PC} = 14.7$ Hz, 2/5-C), 139.9 (dd, $J_{PC} = 7.4$, 1.6 Hz, *i*-C), 136.4 (dd, $J_{PC} = 3.2$, 1.6 Hz, *o*-C), 129.9 (d, $^4J_{PC} = 1.0$ Hz, *m*-CH), 127.2 (d, $^5J_{PC} = 1.8$ Hz, *p*-CH), 121.1 (dd, $J_{PC} = 8.7$, 1.0 Hz, *N*-CH), 21.4 (d, $^4J_{PC} = 0.5$ Hz, *o*- CH_3), 21.4 (dd, $J_{PC} = 22.1$, 1.0 Hz, CH_2), 20.3 (dd, $^3J_{PC} = 6.4$ Hz, $^4J_{PC} = 3.3$ Hz, CH_2), 18.8 (dd, $^3J_{PC} = 5.3$ Hz, $^4J_{PC} = 2.4$ Hz, CH_3), 17.0 (d, $^4J_{PC} = 1.4$ Hz, CH_3); MS (EI, 70 eV, 400 K) *m/e* (%) 490.3 (0.1) [$M]^+$, 295.1 (100) [$M - C_{12}H_{20}P]^+$, 194.1 (22) [$M - C_{18}H_{21}N_2P]^+$. $C_{30}H_{40}N_2P_2$ (490.61): C 73.45, H 8.22, N 5.71; found C 72.94, H 8.13, N 6.02.

1,3-Dimesityl-2-(3',4'-dimethyl-phospholyl)-dihydro-1,3,2-diazaphosphole 4d. A solution of 3,4-dimethyl-1-trimethylstannylphosphole (2.75 g, 10 mmol) in THF (50 mL) was added dropwise to a cooled (-78 °C) solution of 1,3-dimesityl-2-chloro-dihydro-1,3,2-diazaphosphole (3.60 g, 10 mmol) in THF (100 mL). The solution was then allowed to warm to room temperature and stirred for an additional 1 h at this temperature. The solvent was then removed under reduced pressure, and the residue was dissolved in hexane (100 mL) and filtered over Celite. The filtrate was concentrated under reduced pressure to a total volume of 30 mL and stored at -20 °C for crystallization. The orange colored crystals were collected by filtration and dried in vacuum to yield 3.71 g (85%) of **4d** of mp 131 °C. 1H NMR (C_6D_6) δ 6.79 (s, 4 H, *m*-CH), 6.00 (s, 2 H, $CH_{phosphole}$), 5.89 (d, 2 H, $^3J_{PH} = 0.5$ Hz, *N*-CH), 2.44 (s, 12 H, *o*- CH_3), 2.11 (s, 6 H, *p*- CH_3), 1.85 (s, 6 H, CH_3); $^{13}C\{^1H\}$ NMR (C_6D_6) δ 151.5 (dd, $J_{PC} = 6.9$, 4.0 Hz, *i*-C), 147.4 (d, $^2J_{PC} = 0.7$ Hz, CCH_3), 137.9 (t, $^{12}J_{PC} = 7.1$ Hz, CH), 136.5 (s, *o*-C), 136.1 (s, *p*-C), 130.5 (d, $^4J_{PC} = 1.3$ Hz, *m*-C), 120.7 (d, $^2J_{PC} = 8.3$ Hz, *N*-CH), 20.9 (s, *p*- CH_3), 19.7 (s, *o*- CH_3), 17.6 (d, $^3J_{PC} = 1.8$ Hz, CH_3); $C_{26}H_{32}N_2P_2$ (434.50) C 71.87, H 7.42, N 6.45, found C 71.48, H 7.53, N 6.44.

1,3-Bis(2',6'-dimethylphenyl)-2-(2',4'-dimethyl-3',5'-diphenylphospholyl)-dihydro-1,3,2-diazaphosphole 4e. Lithium (0.07 g, 10 mmol) was added to a solution of 1-chloro-2,4-dimethyl-3,5-diphenylphosphole (1.49 g, 5 mmol) in THF (20 mL). The mixture

was stirred for 12 h at room temperature before unreacted metal was removed by filtration. The remaining solution was slowly added to a cooled (-78 °C) solution of 1,3-bis(2,6-dimethylphenyl)-2-chloro-dihydro-1,3,2-diazaphosphole (1.65 g, 5 mmol) in THF (50 mL). The solution was then allowed to warm to room temperature and stirred for an additional 1 h at this temperature. Solvent was then removed under reduced pressure, and the residue dissolved in toluene (50 mL) and filtered. The filtrate was concentrated under reduced pressure to a total volume of 10 mL and stored at 4 °C for crystallization. The orange colored crystals were collected by filtration and dried in vacuum to yield 2.38 g (85%) of **4e**, mp 212 °C. 1H NMR (C_6D_6) δ 7.27–6.73 (m, 10 H, H_{phenyl}), 6.78 (s, 6 H, *m/p*-H), 5.74 (s, 2 H, *N*-CH), 2.33 (s, 12 H, *o*- CH_3), 2.09 (s, 3 H, 3'- CH_3), 1.47 (dd, 3 H, $^4J_{PH} = 9.6$ Hz, $^5J_{PH} = 2.6$ Hz, 5'- CH_3); $^{13}C\{^1H\}$ NMR (C_6D_6) δ 155.2 (dd, $J_{PC} = 7.2$, 2.2 Hz, *i*-C), 144.5 (d, $^3J_{PC} = 1.4$ Hz, *i*-C), 140.9 (dd, $J_{PC} = 21.2$, 3.3 Hz, $C_{phosphole}$), 140.8 (dd, $J_{PC} = 1.7$, 0.7 Hz, *i*-C), 140.2 (dd, $^1J_{PC} = 24.2$ Hz, $^2J_{PC} = 15.8$ Hz, $C_{phosphole}$), 139.3 (dd, $J_{PC} = 19.3$, 0.4 Hz, $C_{phosphole}$), 139.2 (dd, $J_{PC} = 7.7$, 1.6 Hz, $C_{phosphole}$), 135.8 (dd, $J_{PC} = 3.2$, 1.8 Hz, *o*-C), 130.2 (d, $^5J_{PC} = 0.6$ Hz, *o*-CH), 130.1 (dd, $^3J_{PC} = 8.4$ Hz, $^4J_{PC} = 1.0$ Hz, *o*-CH), 129.4 (d, $^3J_{PC} = 0.8$ Hz, *m*-CH), 128.3 (s, *m*-CH), 127.3 (d, $^5J_{PC} = 1.7$ Hz, *m*-CH), 126.5 (s, *p*-CH), 124.8 (d, $^3J_{PC} = 1.1$ Hz, *p*-CH), 122.0 (dd, $J_{PC} = 8.3$, 1.2 Hz, *N*-CH), 19.9 (dd, $^3J_{PC} = 5.6$ Hz, $^4J_{PC} = 3.2$ Hz, 3'- CH_3), 16.9 (s, *o*- CH_3), 14.6 (dd, $J_{PC} = 24.6$, 1.5 Hz, 5'- CH_3); MS (EI, 70 eV, 470 K) *m/e* (%) 295.1 (100) [$M - C_{18}H_{16}P]^+$, 264.1 (36) [$C_{18}H_{17}P]^+$. $C_{36}H_{36}N_2P_2$ (558.64): C 77.40, H 6.50, N 5.01; found C 77.12, H 6.63, N 5.04.

Crystallography. The crystal structure determinations were performed on a Nonius Kappa-CCD diffractometer at 123(2) K (**4b,d–f**) or on a Bruker Kappa-APEXII diffractometer at 173(2) K (**4c**) using Mo $K\alpha$ radiation ($\lambda = 0.71073$ Å). Crystal data, data collection parameters, and results of the analyses are listed in Table 1 and selected metrical parameters in Table 2. Direct methods (SHELXS-97)⁴⁷ were used for structure solution, and refinement was carried out using SHELXL-97 (full-matrix least-squares on F^2).⁴⁷ Hydrogen atoms were refined using a riding model. CCDC-725355 (**4b**), CCDC-725356 (**4c**), CCDC-725357 (**4d**), CCDC-725358 (**4e**), and CCDC-725359 (**4f**), contain the supplementary crystallographic data for this paper. These data can be obtained free of charge from The Cambridge Crystallographic Data Centre via www.ccdc.cam.ac.uk/data_request/cif.

Acknowledgment. We thank Dr. J. Opitz, J. Trinkner, and K. Wohlbold (Institut für Organische Chemie, Universität Stuttgart) for recording the mass spectra. The Deutsche Forschungsgemeinschaft is acknowledged for financial support. M.N. thanks the DAAD for financial support.

Supporting Information Available: CIF files giving X-ray structural information on **4b–f**, full ref 39, coordinates and energies of optimized molecular structures of **7** at various levels of theory, plots of interplanar angle ϕ and P-centered bond angles of **4a–f** versus r_{PP} , and plots illustrating the temperature dependence of $^1J_{PP,soln}$. This material is available free of charge via the Internet at <http://pubs.acs.org>.

JA903156P

(47) Sheldrick, G. M. *Acta Crystallogr.* **2008**, *A64*, 112.